Computer Optics Vol. 2, No. 1, pp. 39–51, 1990
Printed in Great Britain

0955–355X/90 $10.00 + 0.00

NUMERICAL ANALYSIS OF SPATIAL STRUCTURE OF COHERENT OPTICAL WAVE FIELDS

A. V. KOBYSHEV, E. V. KURMYSHEV and I. N. SISAKYAN

Abstract—Computer programs developed for numerical evaluation of the Kirchhoff integral for the case of planar optical elements of arbitrary shape were thoroughly tested. The spatial distribution of diffracted wave fields was investigated as a function of shape of planar optical elements and Gaussian inhomogeneities in the irradiance of the illuminating beam. For the axially symmetric problem, analytical representations of the diffraction integral were obtained in the Fraunhofer and Fresnel approximations as a series in Bessel functions. These representations proved to be convenient in studying the asymptotic effect of inhomogeneities in the intensity of the incident beam. The wave field structure was investigated in the neighbourhood of a geometrical optics parabola, a point focus, and an axial segment with uniform distribution of irradiance.

1. INTRODUCTION

To design planar optical elements one relies on solving the direct problem of wave theory, i.e. the evaluation of the distribution of the wave field in a certain region of space when given the distribution of the field and/or its derivatives at the boundary of this region. The computer programs and algorithms to solve this problem may be viewed as building blocks of a computer-assisted system of planar optics design [1, 2].

For the inverse problem of field focusing into a specified region of space so as to achieve a desired distribution of intensity, three methods of solution have been elicited [3, 4]. The first method, widely accepted and well-developed mathematically, relies upon the geometrical optics approximation [3, 5, 6]. The second approach takes diffraction effects into account and reduces to a minimization problem for the respective functionals of a residual, and is usually handled by iterative techniques [3, 4]. The third method of focuser synthesis boils down to solving a nonlinear [7] or linear integral equation which relates the distribution of the phase or the field at the focuser to the desired distribution of intensity in the focal plane.

Solution of the direct diffraction problem is then a necessary means of verifying and refining the solutions of the inverse ill-posed problem. Direct verification of an inverse solution is especially desirable when it is difficult or even impossible to prove the convergence of the algorithm, the uniqueness of the solution, or the very existence of a solution when handling a certain class of functions. These difficulties, among increasing demands for corrector plates and focusers of coherent wave fields, and their strict design specifications have motivated the development of efficient programs that provide a detailed investigation in the spatial structure of the wave fields formed by these optical elements wherever diffraction effects are involved [17].

In this work we used familiar computational algorithms [8] to develop programs computing the two-dimensional Kirchhoff integral for the case of planar focusers of arbitrary shape. These programs were subjected to a detailed testing to reveal the domain of the applicability. The structure of the wave field was obtained in the vicinity of the geometrical optics parabola, a focal point, and an axial section at a place of uniform intensity. The spatial distribution of wave fields was studied as a function of the shape of planar optical elements with allowance for Gaussian inhomogeneities of illumination.

2. MATHEMATICAL PROBLEM STATEMENT (KIRCHHOFF INTEGRAL)

This section sets out the direct problem [9, 10], thus providing a basis for subsequent discussion. Suppose that the propagation of a monochromatic wave in a homogeneous isotropic medium is described by the wave function $U(P, t) = U(P)\exp(i\omega t)$ which satisfies the wave equation and the

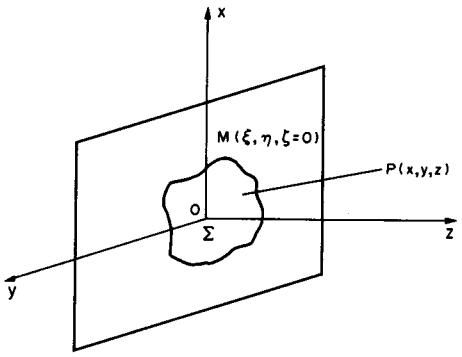

Fig. 1. Geometry of the problem.

complex wave field $U(P)$ satisfies the Helmholtz equation

$$\Delta U + k^2 U = 0, \tag{1}$$

where $k = 2\pi/\lambda$ is the wavenumber, and $P(x, y, z)$ is a point with coordinates x, y, z in physical space.

Let the optical element occupying a domain in the plane $z = 0$ (Fig. 1) be illuminated by a wave $U(\xi, \eta, 0-0)$. This element transforms this wave into another wave $U(\xi, \eta, 0+0) = G(\xi, \eta)U(\xi, \eta, 0-0)$, where $G(\xi, \eta)$ is the complex transmittance of the planar element. If $|G| = 1$ this is a purely phase element, if Im $G = 0$ this is a purely amplitude element, and in the general case one may consider amplitude-phase elements with an arbitrary complex function $G(\xi, \eta)$. Notice that the polarization effects are not included here. The field behind the element, in the $z \geqslant 0$ half-space, is given by the solution of the appropriate boundary problem for Eq. (1). For the first boundary problem (field at the boundary is given), the solution to Eq. (1) may be represented with the aid of the Green function [9, 10] as

$$\begin{aligned} U(P) &= \frac{k}{2\pi i} \int\int_{S_1} U(\xi, \eta, 0+0) \frac{z}{r} \frac{e^{ikr}}{r} \, d\xi \, d\eta \\ &= \frac{k}{2\pi i} \int_{\Sigma} \varphi(\xi, \eta) \frac{z}{r} \frac{e^{ikr}}{r} \, d\xi \, d\eta \\ &\quad + \frac{k}{2\pi i} \int\int_{S_1/\Sigma} U(\xi, \eta, 0) \frac{z}{r} \frac{e^{ikr}}{r} \, d\xi \, d\eta \\ &\simeq \frac{k}{2\pi i} \int\int_{\Sigma} \varphi(\xi, \eta) \frac{z}{r} \frac{e^{ikr}}{r} \, d\xi \, d\eta, \end{aligned} \tag{2}$$

where S_1 is the plane $z = 0$, $r^2 = (x-\xi)^2 + (y-\eta)^2 + z^2$, it is assumed that $kr \gg 1$, and $\varphi(\xi, \eta) \equiv U(\xi, \eta, 0+0)$ for $M(\xi, \eta) \in \Sigma$.

It is worth noting that high accuracy is required in the treatment of the boundary conditions when in (2) one changes the integration from over the whole of plane S_1 to that over domain Σ. This is especially true in formulating the inverse problem when the field at the boundary is evaluated from the distribution in a particular space. Indeed, an actual amplitude-phase element has finite dimensions and may be fitted into an opaque screen, or illuminated by an unconfined beam, or be a combination of these situations. Then, the transition in (2) from the integration domain S_1 to Σ implies in mathematical terms that a field $\varphi(M)$ is given such that $\varphi(M) \equiv U(M, 0+0)$ for $M \in \Sigma$ and $\varphi(M) = 0$ for $M \in S_1 \setminus \Sigma$. These are the approximate Kirchhoff boundary conditions for the first boundary value problem.

When the element is mounted in an opaque screen, this implies that in Eq. (2) the contribution of the field $U(M \in S_1 \setminus \Sigma, 0+0)$ beyond the boundary is neglected, i.e. the field $U(M, 0+0)$ is assumed to fall off rapidly outside the screen. For the inverse problem this implies that fields $U(M, 0+0)$ with infinite carrier wave are allowed as solutions provided that these fields rapidly decay outside the focuser. If the element is illuminated by an unconfined beam, the approximate

Kirchhoff boundary conditions allow the solution of the first boundary value problem accurate to the contribution of the field $U(M \in S_1 \setminus \Sigma, 0+0)$ only.

Two approximations of the Kirchhoff integral are in wide use [9]. In the Fresnel approximation,

$$U(P) = \frac{\exp(ikz)}{i\lambda z} \exp\left(i\pi \frac{x^2+y^2}{\lambda z}\right) \int\int_{\Sigma} (\xi, \eta) \exp\left(i\pi \frac{\xi^2+\eta^2}{\lambda z}\right) \exp[-i2\pi(f_x\xi + f_y\eta)]\, d\xi\, d\eta, \quad (3)$$

where $f_x = x/(\lambda z)$, and $f_y = y/\lambda z$.

If a is the radius or characteristic dimension of the aperture, then the region of Fresnel diffraction corresponds to the wave parameter $D = \lambda z/\pi a^2$ being close to unity, and $|x-\xi| \ll 1$, $|y-\eta| \ll 1$, $r \simeq z + 0.5[(x-\xi)^2 + (y-\eta)^2]$; while the region of Fraunhofer diffraction is consistent with $D \gg 1$, $\exp[i\pi(\xi^2+\eta^2)/\lambda z] \approx 1$ and the field is given as

$$U(P) = \frac{e^{ikz}}{i\lambda z} \exp\left(i\pi \frac{x^2+y^2}{\lambda z}\right) \int\int_{\Sigma} \varphi(\xi, \eta) \exp -i2\pi(f_x\xi + f_y\eta)\, d\xi\, d\eta. \quad (4)$$

Solutions (3) and (4) possess an obvious reciprocity defined by the correspondence of the aperture function $\varphi \leftrightarrow \tilde{\varphi} \equiv \varphi \exp[i\pi(\xi^2+\eta^2)/\lambda z]$.

In this work the Kirchhoff integral was computed by Gaussian quadrature, Simpson's rule, and the trapezium rule written in FORTRAN. A comparison of the results of preliminary computations and an assessment of the numerical evaluation in Lesson *et al.* [11] led to our choosing the computational scheme for the Kirchhoff integral (2) over an arbitrary plane area Σ (unless indicated otherwise, all the following results were determined by Simpson's rule [8] on a VAX-type computer). Incidentally, it may be noted that even in the axially symmetric problem we did not resort to any relevant simplifications, such as addition in rings, and we used a single computational scheme suitable for an arbitrary plane area throughout the whole study.

3. EXAMPLES OF KIRCHHOFF INTEGRAL EVALUATION

3.1. *Diffraction of a plane wave at circular and elliptical apertures*

In the Fraunhofer approximation, a uniform plane wave $U = A e^{ikz}$ ($A = \text{const.}$, $\text{Im}\, A = 0$), diffracted by a circular aperture of radius a is described by Eq. (4) at $\varphi(\xi, \eta) = A$. This integral is amenable to an easy analytic calculation and the distribution of intensity of the diffracted wave in the observation plane $z = z_0$ is given by the familiar expression [9, 12]

$$I(R, z) = |U(R, z)|^2 = I(0, z)\left(\frac{2J_1(kaR/z)}{kaR/z}\right)^2, \quad (5)$$

where $I(0, z) = (A/D)^2$ is the intensity along the z-axis, the wave parameter $D = \lambda z/(\pi a)^2 \gg 1$, λ is the operating wavelength, and $R^2 = x^2 + y^2$.

The numerical integration by Eq. (2) with $\varphi(\xi, \eta) = A$, $a = 10^{-2}$ m, $\lambda = 0.6328 \times 10^{-6}$ m and $z = 5 \times 10^3$ m (which corresponds to $D \simeq 10$) produced a result that agrees with that of Eq. (5) accurate to the 4th decimal place, using a mesh of only 64×64 nodes. The time to compute the field at one observation point was 3.6 s.

Changing the coordinates in the aperture plane $z = 0$ as $\xi' = \mu_x\xi$ and $\eta' = \mu_y\xi$ (μ_x and μ_y are real-valued constants) maps the aperture Σ into Σ'. In the Fraunhofer approximation, Eq. (4) readily yields a congruence relation for the diffraction of a plane wave at apertures Σ and Σ' [12]. For the intensity of the diffracted waves, this congruence is written as

$$I(x, y, z) = \mu_x\mu_y)^{-2} I'(x', y', z'), \quad (6)$$

where $x' = x/\mu_x$ and $y' = y/\mu_y$. In other words, the intensity I' of a plane wave diffracted by a hole as measured at a point (x', y', z') is $(\mu_x\mu_y)^2 I(\mu_x x', \mu_y y', z)$. Equation (6) was used as one of the checking relations for the program computing the integral (2).

The distribution of field intensity was also computed for a plane wave diffracted at elliptical apertures $\xi'^2/\mu_x^2 + \eta'^2/\mu_y^2 = a^2$ with a semi-axis ratio of $\mu_x/\mu_y = 1$, 1.01 and 1.5. For simplicity of comparison it was required that $\mu_x\mu_y = 1$, while the values of a, λ and z were kept the same as for the circular aperture case. The results of calculations at the corresponding points were found to be in full agreement with Eq. (6).

3.2. *The focal spot*

Let us investigate the diffraction of a converging spherical wave at circular and elliptic apertures. The spherical wave converges to the focal point $P(0, 0, z_0)$ at the z-axis. In the aperture plane its amplitude-phase distribution is

$$\varphi(\xi, \eta) = A \exp(-ik\sqrt{z_0^2 + \xi^2 + \eta^2})/\sqrt{z_0^2 + \xi^2 + \eta^2}$$
$$\simeq (A/z_0) \exp[-kz_0(1 + (\xi^2 + \eta^2)/2z_0^2)], \tag{7}$$

where z_0 is the focal length of the lens, A is a real valued constant, and it is assumed that if the characteristic linear dimension of the aperture is a, then $a/z_0 \ll 1$.

The numerical evaluation of the Kirchhoff integral (2) with the aperture function (7) was carried out for a number of elliptical apertures $\{\sum_{ij}: \xi^2/\mu_{xj}^2 + \eta^2/\mu_{yj} = a_i^2;\ i,j = 1, 2, 3\}$. For each value of a_i from the set $(a_1, a_2, a_3) = 0.5$ mm, 1 mm and 1.5 mm, the semi-axis ratio $\mu_j = \mu_{xj}/\mu_{yj}$ took on all values from the set $(\mu_1, \mu_2, \mu_3) = (1, 1.01, 1.5)$. For simplicity of comparison of the results it was always required that $\mu_{xj}\mu_{yj} = 1$, that is, the areas $S_i = 4\pi a_i^2$ of apertures $\sum_{ij}$ were independent of μ_j. Some computations on the mesh of 128×128 nodes are summarized in the tables and figures of this paper. We note that the time to compute the integral (2) at each point of observation amounted to about 14 s.

Figure 2 shows the relative intensity distributions $\tilde{I}(x, y, z_0) \equiv I_{1j}(x, y, z_0)/I_{1j}(0, 0, z_0)$ of the light field in the focal plane $z = z_0$, along the axes z and y (for the circular aperture of $\mu_1 = 1$, the distribution is axially symmetric).

For a circular aperture ($\mu_1 = 1$), the first minimum $\tilde{I}_{11}(R_{11\min}, z_0) = 8 \times 10^{-4}$ is achieved at the circle of radius $R_{11\min} = 8 \times 10^{-5}$ m (127λ). For an elliptical aperture with $\mu_2 = 1.01$, the first minimum $\tilde{I}_{12}(x_{12\min}, 0, z_0) = 4 \times 10^{-4}$ of the intensity distribution along the x-axis is achieved at $x_{12\min} \simeq \pm 7.5 \times 10^{-5}$ m ($\simeq 118\lambda$), while the distribution along the y-axis attains its first minimum $\tilde{I}_{12}(0, y_{12\min}, z_0) \simeq 5.9 \times 10^{-4}$ at $y_{12} = \pm 8.5 \times 10^{-5}$ m ($\simeq 133\lambda$).

For a weakly elliptic aperture of $\mu_2 = 1.01$, the maximum deviation of the distributions $\tilde{I}_{12}(x, 0, z_0)$ and $\tilde{I}_{12}(0, y, z_0)$ from the function $\tilde{I}_{11}(R, z_0)$ nowhere exceeds a value of about $\sim 10^{-3}$, therefore the plots of these distributions practically coincide in Fig. 2.

For an elliptic aperture with $\mu_3 = 1.5$ we get $\tilde{I}_{13}(x_{13\min}, 0, z_0) = 1.8 \times 10^{-3}$ for $x_{13\min} \simeq \pm 6 \times 10^{-5}$ m ($\simeq 95\lambda$), and $\tilde{I}_{13}(0, y_{13\min}, z_0) = 1.6 \times 10^{-3}$ for $y_{13\min} \simeq \pm 9 \times 10^{-5}$ m ($\simeq 143\lambda$); these data are summarized in Table 1(a, b).

The plots in Fig. 2 reveal that the intensity distributions extend along the y-axis and contract along the x-axis according as the aperture circle contracts in the y-axis and extends along the x-axis when the circle is deformed into the ellipses. This fact obviously agrees with the similarity relation (6), which is not obeyed strictly in this particular case, however.

Figure 3 shows the relative intensity distributions $\tilde{I}_{ij}(0, 0, \Delta z) \equiv I_{ij}(0, 0, \Delta z)/I_{1j}(0, 0, z_0)$ along the z-axis near the focus z_0, so that $\Delta z = z - z_0$. Notice the shift of the maxima $I_{1j}(0, 0, \Delta z_{1j\max})$ from

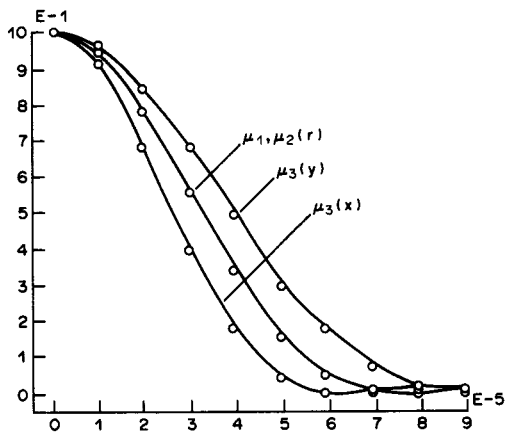

Fig. 2. Spherical wave. Distribution of intensity in the focal plane: $a_1 = 5$ mm, $\mu_1 = 1, \mu_2 = 1.01, \mu_3 = 1.5$.

Table 1(a). $x_{ij,\min}$, top rows, and $y_{ij,\min}$ ($\times 10^{-5}$ m)

	μ_1	μ_2	μ_3
a_1	8 (127λ)	7.5 (118λ)	6 (95λ)
	8 (127λ)	8.5 (133λ)	9 (143λ)
a_2	3.8 (60λ)	3.8 (60λ)	3.2 (50λ)
	3.8 (60λ)	3.8 (60λ)	4.8 (75λ)
a_3	1.9 (30λ)	1.9 (30λ)	1.6 (25λ)
	1.9 (30λ)	1.9 (30λ)	2.4 (38λ)

Table 1(b). $\tilde{I}_{ij}(x_{ij,\min}, 0, z_0)$, top rows, and $\tilde{I}_{ij}(0, y_{ij,\min}, z_0)$

	μ_1	μ_2	μ_3
a_1	8×10^{-4}	4×10^{-4}	1.8×10^{-3}
	8×10^{-4}	5.94×10^{-4}	1.6×10^{-3}
a_2	1.6×10^{-4}	7.7×10^{-5}	1.4×10^{-4}
	1.6×10^{-4}	2.7×10^{-4}	1.5×10^{-4}
a_3	1.68×10^{-4}	7.9×10^{-5}	1.4×10^{-4}
	1.68×10^{-4}	2.8×10^{-4}	1.5×10^{-4}

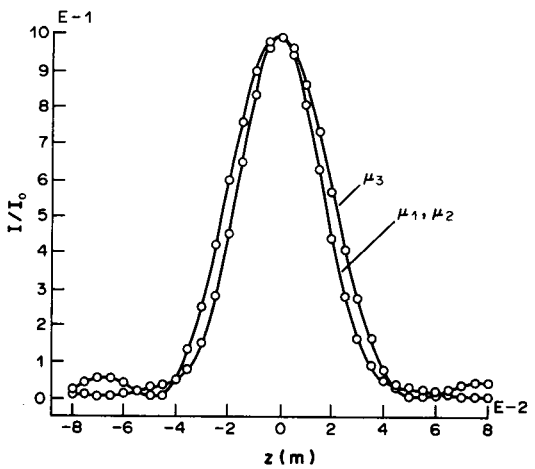

Fig. 3. Spherical wave. Distribution of intensity on the z-axis. $a_1 = 5$ mm, $u_1 = 1$, $u_2 = 1.01$, $u_3 = 1.5$.

the focal plane $z = z_0$ toward the aperture (Table 2). The strength and position of the first minima ahead of the focal plane $z = z_0$ and behind it are summarized in Table 3(a, b). These data reveal an appreciable asymmetry about the focal plane of the intensity distribution along the z-axis. This result can be demonstrated analytically for the case of the integral (4) with $\varphi(\xi, \eta)$ given by Eq. (7), although a contrary statement may be found for example in Born and Wolf [12].

In view of the qualitative similarity of the results obtained for the aforementioned values of a_i we do not present the plots for $\tilde{I}_{2j}(x, y, z)$ and $\tilde{I}_{3j}(x, y, z)$, but summarize the characteristic parameters of the distributions for all a_i and μ_j $(i, j = 1, 2, 3)$ in Tables 1–3. Table 1(a) gives the positions $x_{ij\min}$ and $y_{ij\min}$ of the first minima in the distributions $\tilde{I}_{ij}(x, 0, z)$ and $\tilde{I}_{ij}(0, y, z_0)$ respectively along the x- and y-axes. The intensities at these minima, $\tilde{I}_{ij}(x_{j\min}, 0, z_0)$ and $\tilde{I}_{ij}(0, y_{ij\min}, z_0)$, are presented in Table 1(b). In Table 1, the upper rows correspond to the distribution along the x-axis, and the lower rows along the y-axis. Table 2 shows the positions of maxima, $\Delta z_{ij\max}$, in the distributions $\tilde{I}_{ij}(0, 0, \Delta z)$. Table 3(a) gives the positions of first minima, $\Delta z^{(-)}_{ij\min}$ and $\Delta z^{(+)}_{ij\min}$, in the intensity distribution $\tilde{I}_{ij}(0, 0, \Delta z)$ along the z-axis in the vicinity of the focus $z = z_0$. The respective intensities of these minima are summarized in Table 3(b). The upper values in each cell of Table 3 correspond to positions ahead of the focal plane, the lower rows to positions behind the focus.

Table 2. $\Delta/z_{ij,\max}$ (m)

	μ_1	μ_2	μ_3
a_1	-6×10^{-4} (952λ)	-8×10^{-4} (126λ)	-5.1×10^{-3} (8057λ)
a_2	-5×10^{-5} (8λ)	-6×10^{-5} (95λ)	-3×10^{-5} (47λ)
a_3	-3×10^{-6} (5λ)	-3×10^{-6} (5λ)	-2×10^{-5} (31λ)

Table 3(a). $\Delta z_{ij,\min}^{(-)}$, top rows, and $\Delta z_{ij,\min}^{(+)}$ (m)

	μ_1	μ_2	μ_3
a_1	-5×10^{-2}	-5×10^{-2}	-6.5×10^{-2}
	5.5×10^{-2}	5.5×10^{-2}	7.5×10^{-2}
a_2	-1.2×10^{-2}	-1.3×10^{-2}	-1.7×10^{-2}
	1.2×10^{-2}	1.3×10^{-2}	1.8×10^{-2}
a_3	-3.2×10^{-3}	-3.2×10^{-3}	-4.4×10^{-3}
	3.2×10^{-3}	3.2×10^{-3}	4.4×10^{-3}

Table 3(b). $I_{ij}(0, 0, \Delta z_{ij,\min}^{(-)})$, top rows, and $I_{ij}(0, 0, \Delta z_{ij,\min}^{(+)})$

	μ_1	μ_2	μ_3
a_1	1.5×10^{-3}	1.58×10^{-3}	5×10^{-3}
	7×10^{-4}	7.3×10^{-3}	3.7×10^{-3}
a_2	4.4×10^{-3}	1.5×10^{-3}	4.1×10^{-3}
	1.8×10^{-3}	1.8×10^{-3}	4.6×10^{-3}
a_3	5.6×10^{-5}	5.6×10^{-5}	4.3×10^{-3}
	2×10^{-4}	2×10^{-4}	4.3×10^{-3}

It is worth noting that for a given μ_j an increase in a_i leads to a concentration of the focal spot in all the axes, and there is evidence of a trend towards restored symmetry about the focal plane $z = z_0$.

3.3. *A plane inhomogeneous wave with a Gaussian distribution of amplitude*

In applications, light beams often exhibit inhomogeneous distributions of intensity either for generic reasons (single mode lasing, for example) or due to random stationary distortions of the field. It is essential therefore to estimate and take into account the errors introduced by field inhomogeneities of the incident wave in the focusing by elements designed for plane homogeneous waves. This section will now take as a model problem the effect of a Gaussian amplitude inhomogeneity on the diffraction of a plane wave by a circular aperture.

In the Fresnel approximation (3), the intensity of a plane wave with Gaussian amplitude inhomogeneity, $\varphi(\xi, \eta) = A \exp[-(\xi^2 + \eta^2)/b^2]$, diffracted at a circular aperture, is described by the integral

$$\tilde{I} = \int_0^1 \rho J_0(v\rho) \exp\left(-\frac{u}{2}\rho^2\right) d\rho, \tag{8}$$

where

$u(R, z) = -i2(A/D) \exp(ikz) \exp(ikR^2/2z)\tilde{I}(u, v)$,
$v = kaR/a = 2R/DA$,
$u = 2(a^2/b^2 - iD^{-1})$,
a is the aperture radius,
b is the real valued parameter of the Gaussian distribution,
$D = \lambda z/\pi a^2$ is the wave parameter, and
J_0 is the Bessel function of order zero.

Integration by parts using the familiar equations for Bessel functions leads us to two equivalent representations of the integral (8) as series in powers of the ratio (v/u) or (u/v) with the Bessel functions as coefficients, *viz.*

$$\tilde{I}(u, v) = v^{-1} \exp\left(-\frac{u}{2}\right) \sum_{n=0}^{\infty} \left(\frac{u}{v}\right)^n J_{n+1}(v), \tag{9}$$

$$\tilde{I}(u, v) = u^{-1}\left\{\exp(-v^2/2u) - \exp(-u/2) \sum_{n=1}^{\infty} \left(-\frac{v}{u}\right)^n J_n(v)\right\}. \tag{10}$$

The expressions (9) and (10) are useful analytical estimators of the obtained field (8) as it depends on the behaviour of the inhomogeneity parameter (a/b) and parameter D. They are Neumann's series [13] and may be demonstrated to possess infinite radii of convergence, i.e. converge at any values of u and v.

Given the values of D and a/b, Eqs (9) or (10) readily yield the field (8) on the axis $(R \to 0)$ as

$$\lim_{R \to 0} \tilde{I}(u, v) = u^{-1}[1 - \exp(-u/2)]. \tag{11}$$

According to Eq. (8) the field intensity is given by

$$\begin{aligned} I(R, z) &= |u(R, z)|^2 \\ &= (A/D)^2 4|\tilde{I}(u, v)|^2. \end{aligned} \tag{12}$$

For a diffracted quasi-homogeneous wave, the intensity at the axis results from (11) and (12) as $\lim_{(a/b)\to 0} \lim_{R\to 0} \tilde{I}(u, v)$, namely,

$$I_u(0, z) = (A/D)^2 4D^2 \sin^2(1/2D). \tag{13}$$

In the Fraunhofer approximation of $D \gg 1$, Eq. (13) gives the known value $I_u(0, z) = (A/D)^2$.

The effect of nonuniformity a/b on the field intensity on the axis may be readily estimated by Eq. (11) in the Fraunhofer approximation

$$\begin{aligned} I(0, z)|_{D\gg 1} &= (A/D)^2 (a^2/b^2)^{-2}[1 - \exp(-a^2/b^2)]^2 \\ &= (A/D)^2, && \text{for} \quad a/b \ll 1, \\ &= (A/D)^2 (a^2/b^2)^{-2} \ll (A/D)^2, && \text{for} \quad a/b \gg 1. \end{aligned} \tag{14}$$

This expression suggests that for given parameters A and D an increasing inhomogeneity a/b entails a monotonous fall of field intensity on the axis, which might be associated with the drop of the energy integral $\int |\varphi(\xi, \eta)|^2 \, d\xi \, d\eta$ for the incident beam.

For an appreciable nonuniformity $a/b \gg 1$, a given value of parameter D (which corresponds to large values of variable u), and moderate values of v, the Bessel functions in (10) may be developed in the variable to get

$$\tilde{I}(u, v) = u^{-1}[1 - \exp(-u/2)] \exp(-v^2/2u).$$

Consequently, like in the near field $(D \sim 1)$, for the far field case of $D \gg 1$ and $a/b \gg 1$, Eq. (12) yields an exponential intensity distribution in R, *viz.*

$$I_{nu}(R, z) \simeq \left(\frac{A}{D}\right)^2 \left(\frac{a^2}{b^2}\right)^{-2} \exp\left(-\frac{2R^2}{D^2 a^2 (a^2/b^2)}\right), \tag{15}$$

which coincides with Eq. (14) at $R = 0$.

For a weak inhomogeneity $a/b \lesssim 1$ and not very small $D \gtrsim 1$, retaining the leading term in (9) we have

$$\tilde{I}(u, v) = \exp(-u/2) v^{-1} J_1(v) + O(v^{-2} J_2(v) \exp(-a^2/b^2)). \tag{16}$$

It should be emphasized that the remainder

$$O(|u| v^{-2} J_2(v) \cdot \exp(-a^2/b^2)) \sim \exp(-a^2/b^2) 2[(a^2/b^2)^2 + D^{-2}]^{-1/2}$$

will be sufficiently small even at $a/b \simeq 1$ because the growth of $|u|$ with an increase of inhomogeneity

a/b is outbalanced by the fall of $\exp(-a^2/b^2)$. Consequently, the functional form (16) of the integral $\tilde{I}(u, v) = \exp(-u/2)v^{-1}J_1(v)$ will be valid not only for $D \gg 1$ and $a/b \ll 1$ but also for the relaxed conditions $D \gtrsim 1$ and $a/b \lesssim 1$. The field in this case is defined by the expression

$$I(R, z) = (A/D)^2 \exp(-2a^2/b^2)[2v^{-1}J_1(v)]^2. \tag{17}$$

We give, one more way to derive the expressions (15)–(17) for the Fraunhofer approximation of $D \gg 1$. In this case, given a weak inhomogeneity $a/b \ll 1$ the integral (8) takes the form

$$\tilde{I}(u, v) = \tilde{I}(0, v) = \int_0^1 \rho J_0(v\rho)\,\mathrm{d}\rho = v^{-1}J_1(v)$$

that corresponds to the formula (17).

For $D \gg 1$ and a strong inhomogeneity, $a/b \gtrsim 1$, the upper limit of integration in (8) may be extended to infinity and we arrive at the expression

$$\begin{aligned}\tilde{I} &= \int_0^1 \rho J_0(v\rho) \exp\left(-\frac{a^2}{b^2}\rho^2\right)\mathrm{d}\rho \\ &\sim \int_0^\infty \rho J_0(v\rho) \exp\left(-\frac{a^2}{b^2}\rho^2\right)\mathrm{d}\rho \\ &= \frac{1}{2}(a^2/b^2)^{-1} \exp\left(-\frac{v^2}{4a^2/b^2}\right)\end{aligned}$$

corresponding to Eq. (15).

The computations of the Kirchhoff integral (2) for various cases of a plane inhomogeneous wave $\varphi(\xi, \eta) = A \exp[-(\xi^2 + \eta^2)/b^2]$ diffracted by a circular aperture of radius a are plotted in Fig. 4(a,b). These results agree completely with the conclusions of the preceding analysis. Indeed, for $D = 10$ (Fig. 4a) and for $D = 1$ (Fig. 4b), the radial intensity plots are well described, up to nonuniformities $(a/b)_i \lesssim 1$, by the dependence $I/I_0 \sim 4v^{-2}J_1^2(v)$ corresponding to the plane homogeneous wave. The first minimum is located by the zero $3.832 \simeq v_{\min} = 2R/Da$ of the Bessel function $J_1(v)$. Increasing the inhomogeneity $a/b \gtrsim 1$ of the incident beam causes the dependence (17) to reduce monotonously to Eq. (15). Note in passing that for the situations under study, the computation program yielded, in a stable manner, two or three side maxima (minima) of the intensity distribution.

An analysis of the Gaussian amplitude inhomogeneity for the particular case of $D \gg 1$ for a plane inhomogeneous wave diffracted by a circular aperture may be also found in Klimov [16]. This author has obtained a field expansion of the type of Eq. (9), but in another form. For the case in question, Klimov's conclusions agree with those drawn in this section.

3.4. *Wave pattern of the field in geometrical optical focusing into a parabola, point and axial segment*

Substantial advances in the synthesis of optical elements are to a considerable extent associated with the use of geometrical optics [1, 3–6, 14, 15]. However, when the effects of diffraction are taken into account, it is necessary to invoke wave theory to describe operation of optical elements. In this section we resort to the formal Kirchhoff integral (2) to perform a numerical analysis of the wave pattern formed by planar phase elements with the aperture functions $\varphi(\xi, \eta)$ obtained by solving the inverse problem in the approximation of geometrical optics.

For a planar optical element of radius $a = 12.8 \times 10^{-3}$ m and focal length $f = 3 \times 10^{-1}$ m operating at $\lambda = 1.06 \times 10^{-5}$ m and focusing, in the geometrical optics approximation, a plane wave into the segment of parabola $y = x^2/2R$, $x \in [-d, d]$, with $2d = 6 \times 10^{-3}$ m and $R = 5 \times 10^{-2}$ m in the focal plane $z = f$, the aperture function $\varphi(\xi, \eta)$ was computed by formulae borrowed from Danilov *et al.* [14]. The results of the computation of the integral (2) with this aperture function $\varphi(\xi, \eta)$ conducted on a mesh of 512×512 nodes are plotted in Figs 5 and 6. The points are normalized with respect to the intensity $I(0, 0, f)$.

Figure 5 shows the distribution of intensity in the x-axis of the focal plane $z = f$, symmetric about $x = 0$.

It is interesting to analyse the structure of irradiance in the neighbourhood of the geometric

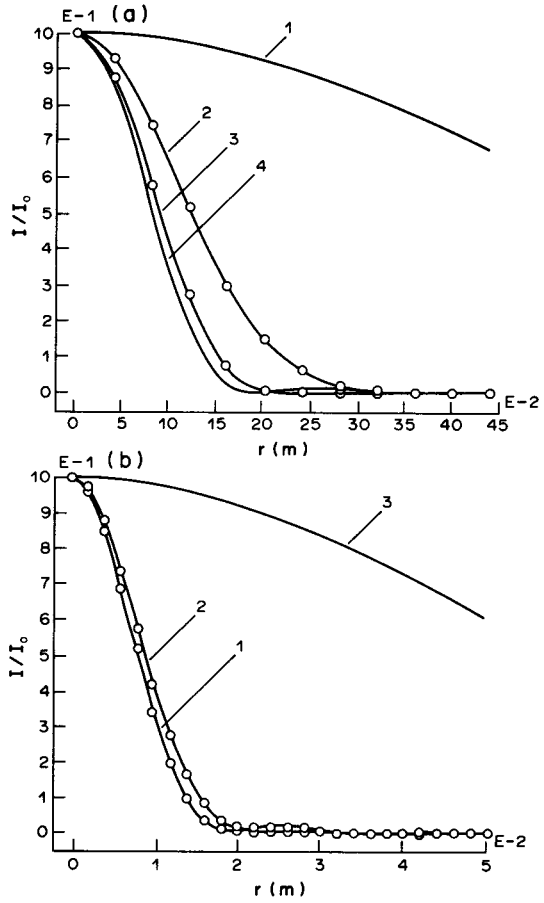

Fig. 4. Radial distributions of relative intensity $I_i(R, z)/I_i(0, z)$: $a = 10$ mm, $\lambda = 632.8$ nm. (a) $D = 10$, $(a/b)_i = 0.1, 1, 2, 10$ for $i = 1, 2, 3, 4$. (b) $D = 1$, $(a/b)_i = 0.1, 1, 10$ for $i = 1, 2, 3$.

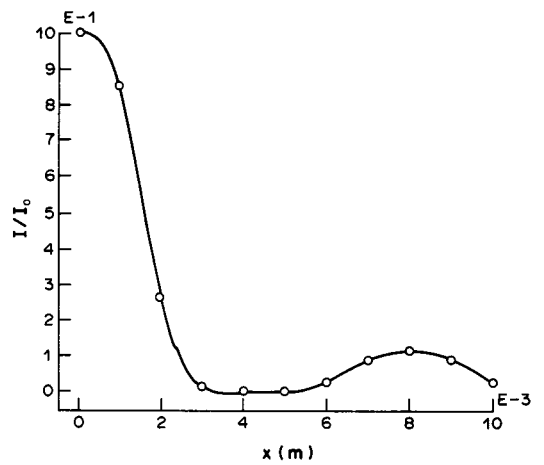

Fig. 5. Focusing into a parabola. Distribution of relative intensity on the x-axis.

parabola $y = x^2/2R$. Figure 6 presents the computation of the field in the focal plane $z = f$ as the distributions of relative intensity along the y-axis for five values of x, namely, 0, 1, 2, 2.5 and 3 mm. The maxima of these plots are displaced from the true geometric values $y_i = x_i^2/2R$, respectively, by $\Delta y_0 = 0$, $\Delta y_1 \simeq 1.12 \times 10^{-5}$ m ($\simeq \lambda$), $\Delta y_2 \simeq 7.54 \times 10^{-5}$ m ($\simeq 7\lambda$), $y_3 \simeq 5.41 \times 10^{-5}$ m ($\simeq 5\lambda$), $\Delta y_4 \simeq 7.96 \times 10^{-5}$ m ($\simeq 8\lambda$), where each $\Delta y_i = y - y_i$.

The wave width of the parabola, controlled by the spacing between the first minima in the

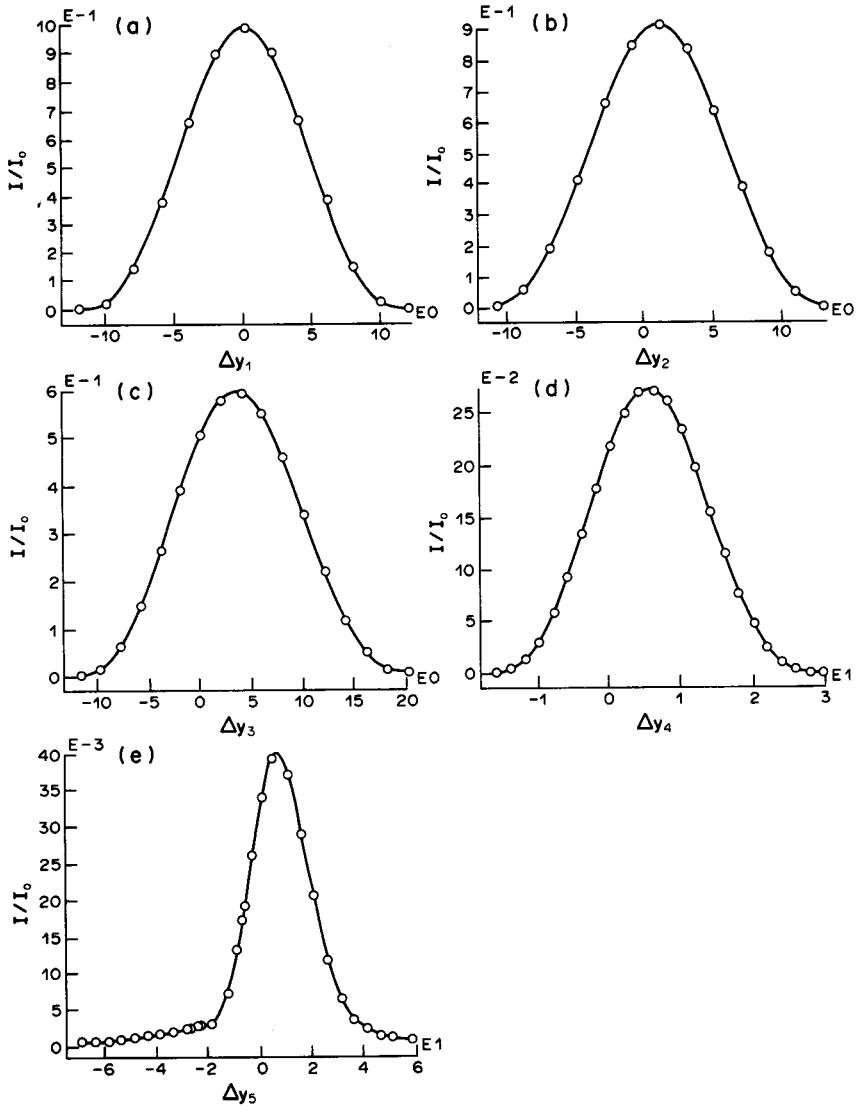

Fig. 6. Focusing into a parabola. Distribution of relative intensity along the axis $\Delta y_i(\lambda)$ in the plane $z = f$ at $\{x_i\} = \{0, 1, 2, 2.5 \text{ and } 3\}$ mm.

distributions shown in Fig. 6, varies from 2.54×10^{-4} m ($\simeq 24\lambda$) at $x_0 = 0$ to 13.46×10^{-4} m ($\approx 127\lambda$) at $x_4 = 3 \times 10^{-3}$ m. The intensity maxima in the distributions in Fig. 6 reduce appreciably near the ends of the parabolae at the above x_i, namely, $\max \tilde{I}(x_0, y) = 1$, $\max \tilde{I}(x_1, y) \simeq 0.921$, $\max \tilde{I}(x_2, y) \simeq 0.579$, $\max \tilde{I}(x_3, y) \simeq 0.274$, and $\max \tilde{I}(x_4, y) \simeq 0.04$. Consequently, the focusing weakens towards the ends of the parabola. This manifests itself in the reduction of maximum intensity and in blurring the focal spot.

The energy integral $\int\int I(x, y, f)\,dx\,dy$ taken over the neighbourhood of the parabola amounts to 84% of the energy of the plane wave incident on the phase element of area $4\pi a^2$.

The calculation of intensity $\tilde{I}(0, 0, \Delta z)$ along the z-axis near $z = f$ indicates that the depth of the parabola, i.e. the spacing between the first minima of the z distribution, amounts to about 3.6×10^{-2} m, and that the intensity maximum is shifted by $\Delta z_{\max} = z_{\max} - f = 3 \times 10^{-4}$ m ($\simeq 30\lambda$) toward the optical element.

Following Danilov *et al.* [14] we let $R \to \infty$ and $d \to 0$ to transform the focal parabola into a point, thus computing the phase function $\varphi(\xi, \eta)$ of the planar optical element that focuses, in the approximation of geometrical optics, a plane wave into a focal point. This phase function was used in computing the integral (2) at a mesh of 128×128 nodes and the same wavelength and focal

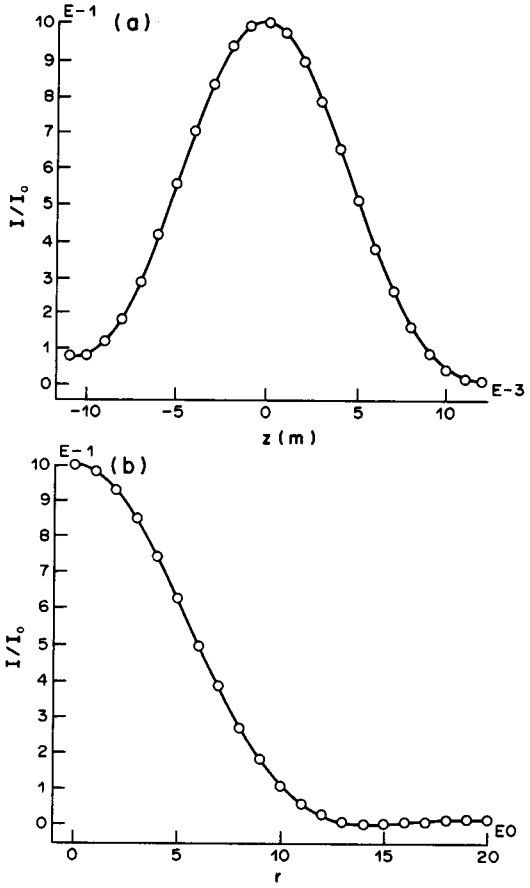

Fig. 7. Intensity distribution of the field in the vicinity of the focal point: (a) on the z-axis, (b) at radius $R(\lambda)$.

length as for the focusing into the parabola. This integral provides insight into the structure of the field in the neighbourhood of the focal point $P(0, 0, f)$.

The maximum of the relative intensity distribution in the z-axis shown in Fig. 7(a) is shifted towards the phase element by $\Delta z_{max} = z_{max} - f = -3 \times 10^{-4}$ m ($\simeq 30\lambda$), while the first minima are at the points $\Delta z^{(-)} \simeq 11 \times 10^{-3}$ m and $\Delta z^{(+)} \simeq 12 \times 10^{-3}$ m, fore and aft of the geometric optical focus. This z distribution is asymmetric both about the focal plane $z = f$ and about z_{max}. In the radial distribution in the focal plane shown in Fig. 7(b), the intensity maximum lies inside the circle of radius $R_{min} \simeq 14\lambda$.

Vasin *et al.* [15] have obtained the transmittance of a phase optical element that focuses, in the geometrical optical approximation, a plane wave into an axial line segment with a uniform distribution of intensity. This transmittance function is

$$(\varphi, \xi) = c^{-1} \ln[-2c\sqrt{\rho^2 + (f + c\rho^2)^2} + 2c^2\rho^2 + 1 + 2fc], \tag{18}$$

where $\rho^2 = \xi^2 + \eta^2$, f is the focal length, $c = \kappa/a^2$, a is the radius of the focuser, and the line segment κ is taken negative if the target zone is ahead of the focus, and positive if behind the focus. For the values of $\lambda = 0.6328 \times 10^{-6}$ m, $f = 3 \times 10^{-1}$ m, $a = 1.28 \times 10^{-2}$ m, and $\kappa = -1.5 \times 10^{-2}$ m borrowed from the paper of Vasin *et al.* [15], we performed the numerical evaluation of the integral (2) with the aperture function (18) to study the wave structure of the field near the axial line segment. The computations were run at two meshes of 256 × 256 and 128 × 128 nodes. The results differ insignificantly, and the subsequent data will be given as those obtained with the former mesh.

Figure 8 shows the z distribution of the relative intensity $\tilde{I}(0, \Delta z) = I(0, \Delta z)/I(0, 0)$ along the optical axis normalized to the intensity $I(0, 0)$ at the focal point ($\Delta z = z - f$). The deviations in

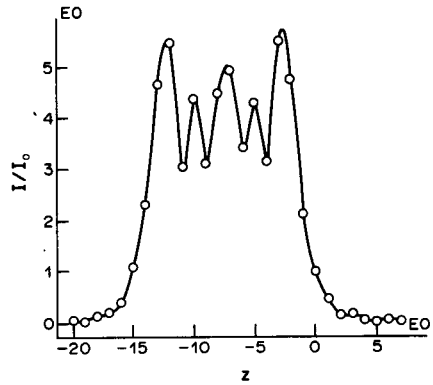

Fig. 8. Focusing into a straight line. Relative intensity variation along the z-axis (dimensions in mm).

the intensity maxima with respect to the level of the uniform distribution

$$\tilde{I}_m = \kappa^{-1} \int_{-1.5}^{0} \tilde{I}(0, z)\,dz \simeq 3.66$$

were as high as 36%.

Figure 9 plots the radial distributions of the relative intensity $\tilde{I}(R, \Delta z) = I(R, \Delta z)/I(0, 0)$ in the planes perpendicular to the z-axis and located at $\Delta z = -15$, -10, -5 and 0 mm (labeled by 1–4, respectively). The wave width, defined as the radius at which the field decays substantially, amounts in the respective sections to $R_{1\min} = 0.7 \times 10^{-4}$ m, $R_{2\min} = 1.9 \times 10^{-4}$ m, and $R_{3\min} \simeq R_{4\min} = 1.4 \times 10^{-4}$ m. The irradiance computed in each of the sections at Δz_k ($k = 1, 2, 3, 4$) from 0 to the radius $R_0 = 10^{-4}$ m as

$$E(\Delta z_k) = 2\pi \int_0^{R_0} I(R, \Delta z_k) R\,dR$$

and normalized to the irradiance of the plane wave incident on the focuser is as follows: $\tilde{E}(\Delta z_1) \simeq 0.15$, $\tilde{E}(\Delta z_2) \simeq 0.41$, $\tilde{E}(\Delta z_3) = 0.51$, and $\tilde{E}(\Delta z_4) = 0.2$.

This evidence indicates that an optical element with transmittance function (18) focuses a plane wave into an axial line segment exhibiting a considerably nonuniform irradiance along the z-axis and noticeable deviations in the R distributions of the field from one cross-section to the next. The radial and z distributions of irradiance represented in Figs 8 and 9 exhibit a qualitative similarity but differ quantitatively from the data of Vasin *et al.* [15]. This discrepancy may be attributed to an approximate procedure when evaluating the Kirchhoff integral as an expansion in Lommel's functions used in the paper of Vasin *et al.* [15].

4. CONCLUSION

A computer program has been developed on the basis of Simpson's rule for evaluating the two-dimensional Kirchhoff integral. An in-depth testing of this program is reported for a wide range of values of the wave parameter and planar optical elements of arbitrary shape. A converging spherical wave diffracted at circular and elliptical apertures produces irradiance patterns asymmetric about the focal plane and about the maximum of the z distribution. This asymmetry tends to decrease for larger apertures. The analytical and numerical analyses of a plane inhomogeneous wave with a Gaussian amplitude inhomogeneity diffracted by a circular aperture indicate that the effect of this inhomogeneity is insignificant in the range $0 \lesssim a/b \lesssim 1$ of the inhomogeneity parameter. This conclusion may be expected to hold, to a certain degree, for elliptical apertures (with the semimajor axis taken for a) and displaced aperture centres and the Gaussian amplitude distribution.

An investigation of the wave structure of the field in the neighbourhood of the geometrical optics parabola, point and axial line segment vividly demonstrates that computer-based synthesis of planar optical elements, in many a situation of practical significance, calls for an essentially wave-theoretical

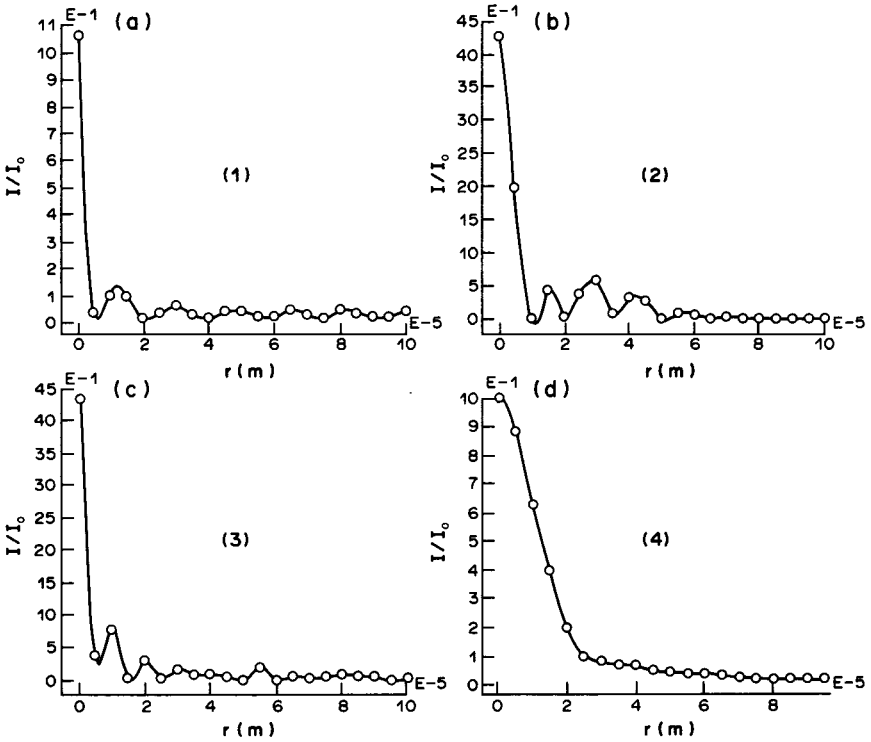

Fig. 9. Focusing into a straight line. Radial distributions of relative intensity at $\{\Delta z_i\} = \{-15, 10, 5 \text{ and } 0\}$ mm.

approach or a step-by-step study of the diffraction effects in solving the inverse problems of optics in the approximation of geometrical optics.

REFERENCES

1. I. N. Sisakyan and V. A. Soifer. Computer-synthesized optics. Problems and advances. *Kompyuternaya Optika* No. 1, 5 (1987). [*Computer Optics* **1**, 3 (1989).]
2. A. E. Berezny, L. I. Brusilovsky, E. A. Otlivanchik *et al.* An automatic system for design, fabrication, and investigation of planar optical elements. Draft 1. *Kompyuternaya Optika* No. 2, 21 (1987). [*Computer Optics* **1**, 163 (1989).]
3. A. V. Goncharsky. Mathematical models in synthesis of planar optical elements. *Kompyuternaya Optika* No. 1, 19 (1987). [*Computer Optics* **1**, 13 (1989).]
4. M. A. Vorontsov, A. N. Matveyev and V. P. Sivokoni. Mode sensitive focuser of laser radiation: design in a diffraction approximation. *Komputernaya Optika* No. 1, 74–78 (1987). [*Computer Optics* **1**, 57 (1989).]
5. A. V. Goncharovsky, V. A. Danilov, V. V. Popov *et al.* Solution of inverse problem of focusing laser radiation into arbitrary curve. *Dokl. Akad. Nauk SSSR* **273** (3), 605 (1983).
6. A. V. Goncharsky, V. A. Danilov, V. V. Popov, I. N. Sisakyan *et al.* Planar focusers of the visible range. *Kvantovaya Elektron.* (Moscow) **13** (3), 660 (1986).
7. N. N. Rozanov and V. E. Semyonov. Formulation of specified profile of irradiation by phase control. *Pisma Zh. Eksp. Teor. Fiz.* **9** (24), 1531 (1983).
8. V. I. Krylov, V. V. Bobkov and P. I. Monastyrsky. *Numerical Methods.* Nauka, Moscow (1976).
9. M. B. Vinogradova, O. V. Rudenko and A. P. Sukhoruchkov. *Wave Theory.* Nauka, Moscow (1979).
10. V. Ya. Arsenin. *Methods of Mathematical Physics and Higher Functions.* Nauka, Moscow (1974).
11. H. A. Lesson, W. V. T. Rusch and H. Schjar-Jacobsen. On numerical evaluation of two-dimensional phase integrals. *IEEE Trans. A.P.* **AP-23** (3), 714 (1975).
12. M. Born and E. Wolf. *Principles of Optics*, 5th edn. Pergamon Press, Oxford (1975).
13. A. Erdelyi (ed.). *Higher Transcendental Functions* (California Institute of Technology, H. Bateman MS Project), 3 vols. McGraw Hill, New York (1953, 1955).
14. V. A. Danilov, V. V. Popov, A. M. Prokhorov *et al.* Optical elements focusing coherent radiation into arbitrary focal curve. *Preprint FIAN* No. 69, Lebedev Physical Institute of the U.S.S.R. Academy of Sciences, Moscow (1983) (in Russian).
15. A. G. Vasin, M. A. Golub, V. A. Danilov, *et al.* Evaluation and investigation of coherent wave field in the focal range of optical elements with rotational symmetry. *Preprint FIAN* No. 304, Moscow (1983) (in Russian).
16. Yu. M. Klimov. *Applied Laser Optics.* Mashinostroyeniye, Moscow (1985).